Medical Microbiology and Immunology (2026) 215:10
https://doi.org/10.1007/s00430-026-00871-5

RESEARCH

The small GTPase Rab5 inhibits actin polymerization mediated by the *Legionella pneumophila* effector VipA

Joana Saraiva[1] · Joana N. Bugalhão[1] · Teresa Carvalho[1,3] · Zach Hensel[3] · Alvaro Crevenna[3] · L. Jaime Mota[1,2] · Irina S. Franco[1,2]

Received: 19 May 2025 / Accepted: 14 March 2026

Abstract

Legionella pneumophila is a facultative intracellular bacterium that causes Legionnaires' disease, one of the most severe manifestations of atypical pneumonia. The capacity of *L. pneumophila* to cause disease relates with its ability to survive and multiply inside a membrane-bound compartment, the *Legionella*-containing vacuole (LCV). The remodeling of the LCV into a replication-competent compartment requires the Icm/Dot type 4 secretion system, that translocates over 300 bacterial effector proteins into host cells. Their action is concerted spatially and timely in order to modulate a multitude of host cell targets and thus ensure LCV segregation from the phagolysosomal pathway. The *L. pneumophila* effector VipA associates with early endosomes and promotes the nucleation of new actin filaments in vitro. Additionally, ectopically produced VipA impairs vesicle trafficking in *Saccharomyces cerevisiae*. However, the mechanisms underlying its association with the endocytic pathway have remained elusive. In this work, we sought the molecular interacting partners of VipA in early endosomes and explored the effects of this association. We found that VipA interacts directly with two key components of these organelles, the membrane lipid phosphoinositide 3-phosphate (PI3P) and the small GTPase Rab5. Binding to Rab5 requires the NH_2-terminal region of VipA but not the COOH-terminal/actin-binding region. Furthermore, binding to Rab5 inhibits VipA-mediated actin polymerization by preventing de novo actin filament formation. These findings offer new insights into the mode of action of VipA and underscore the intricate network of interactions between *L. pneumophila* effectors and their host cell targets, namely in the endocytic pathway.

Keywords *Legionella pneumophila* · Rab5 · PI3P · VipA · Actin polymerization · Endocytic pathway

Introduction

*Legionella pneumophila*is an opportunistic human pathogen responsible for causing Legionnaires Disease, a severe pneumonia that may occur upon the inhalation of contaminated water droplets [1,2]. The pathogen's capacity to initiate infection in alveolar macrophages is driven by selective pressures exerted by its environmental hosts, amoebae [3]. Inside both types of professional phagocytes,*L. pneumophila*resides within a reconfigured compartment known as the*Legionella*-containing vacuole (LCV) that escapes conventional phagosomal maturation. This compartment allows access to essential nutrients, limits inter-bacterial competition and provides protection against complement-mediated lysis and antibody responses. To establish a replication-competent LCV,*L. pneumophila*inhibits phagolysosomal fusion by diverting this compartment from the endocytic pathway [4]. This requires the Icm/Dot type IV secretion

Joana Saraiva and Joana N. Bugalhão have contributed equally to this work.

✉ Irina S. Franco
irinafranco@fct.unl.pt

1 UCIBIO–Applied Molecular Biosciences Unit, Department of Life Sciences, NOVA School of Science and Technology, NOVA University Lisbon, Caparica, Portugal

2 i4HB-Institute for Health and Bioeconomy, NOVA School of Science and Technology, NOVA University Lisbon, Caparica, Portugal

3 Instituto de Tecnologia Química e Biológica, NOVA University Lisbon, Oeiras, Portugal

Published online: 02 April 2026

system that translocates over 300 bacterial effector proteins into host cells, which control a multitude of host cell pathways by acting in a timely and spatially concerted manner [5,6]. The repertoire of effectors presents substantial functional redundancy, meaning that multiple effectors share the same eukaryotic target and consequently are rarely essential for intracellular replication in standard experimental models [7]. Nevertheless, over the past two decades, numerous*L. pneumophila*effectors and their targets have progressively been unravelled and characterized [8–11].

Rab GTPases are key regulators of vesicle trafficking and, together with their regulators and downstream effector proteins, confer organelles their specific identity. Therefore, it is logical that Rab GTPases and related proteins are major targets of intravacuolar pathogens. Rab GTPases alternate between an active GTP-bound form and an inactive GDP-bound state and their interconversion is controlled by the action of Guanine Exchange Factors (GEFs) and GTPase-Activating Proteins (GAPs). GEFs facilitate the replacement of GDP for GTP, allowing Rabs to interact with their effectors and carry out their functions in vesicle formation, movement, and fusion. GAPs in turn increase the intrinsic GTPase activity of Rabs, promoting the conversion from the active GTP-bound state to the inactive GDP-bound state [12]. In particular, endosomal Rab GTPases are manipulated by bacteria to prevent the progressive transfer of endo-lysosomal membrane and luminal constituents to the pathogen-containing vacuoles [2]. For example, Rab5 is a key regulator of endosomal maturation by orchestrating the conversion of early endosomes into late endosomes. Active Rab5 recruits its effector VPS34, a phosphatidylinositol 3-kinase that phosphorylates phosphoinositide (PI) into phosphoinositide 3-phosphate (PI3P), contributing to forming the identity of the early endosomes and to trigger their further maturation into late endosomes [13–16].

The role of Rab5 in the development of the LCV and its modulation by*L. pneumophila*effectors has been addressed in several studies. Rab5 is localized on the surface of the LCV during early stages of host cell infection in both amoebae and macrophages [17,18]. In addition, overexpression of Rab5 is detrimental to*L. pneumophila*replication, likely due to its impact on the integrity of the LCV membrane rather than an increase in lysosomal fusion [17,19–21]. To date, three*L. pneumophila*effectors modulating Rab5 activity have been identified. VipD has a dual Rab5 inhibitory role by preventing its recruitment to early endosomes in the vicinity of the LCV and by blocking the access of Rab5 to a downstream target (early endosomal antigen 1, EEA1), thereby contributing to avoidance of phagosomal maturation [22,23]. Additionally, SidC/SdcA is involved in recruitment of Rab5 to the surface of the LCV and promotes its ubiquitination therein [21] and Lpg0393 is a Rab5 GEF [24]. However, the exact roles of the latter effectors during infection remains uncertain. Thus, despite being a key player in trafficking of the LCV along the phagolysosomal pathway, the mechanisms used by*L. pneumophila*to control the action of Rab5 are mostly unknown.

Our previous studies showed that the*L. pneumophila*effector VipA is an actin nucleator that associates with early endosomes and actin filaments during infection of macrophages, and interferes with vesicle trafficking when ectopically produced in in*S. cerevisiae*.Functional analyses of truncated VipA mutants assigned a fundamental role of its COOH-terminal region (residues 206–339) in actin binding and polymerization, and the requirement of its NH_2-terminal region (residues 1–133) for association with early endosomes. In this work, we investigated its association with these organelles and identified PI3P and Rab5 as the endosomal anchors of VipA. Interaction of VipA with Rab5 is direct, mediated by the NH_2-terminal region of VipA, and hinders the ability of VipA to induce de novo polymerization of actin filaments. These findings provide novel insights on the mode of action of VipA and highlight the complex interplay between*L. pneumophila*effectors and their host cell targets, particularly as modulators of the link between cytoskeleton dynamics and vesicle trafficking.

Materials and methods

Bacterial strains and culture media

Escherichia coli strains used in this work are listed in Table S1 (Supplementary Material) and were routinely grown as previously described [25]. For protein overexpression and Bacterial Two-Hybrid assays see sections below.

Plasmids and oligonucleotides

Plasmids and oligonucleotides used in this study are listed in Tables S1 and S2. For general cloning procedures, restriction enzymes, T4 DNA ligase and Phusion DNA polymerase (Thermo Fisher Scientific) were used according to the manufacturer's instructions. The accuracy of the cloned nucleotide sequences was confirmed by DNA sequencing.

Mammalian cell culture and transfections

CHO FcγRII cells [26] were grown in Dulbecco's Modified Eagle Medium (DMEM; Corning) and 10% (v/v) heat-inactivated fetal bovine serum (FBS; Thermo Fisher Scientific), at 37°C in a 5% (v/v) CO_2 incubator. CHO cells were seeded on 24-well plates at 1×10^5 cells/well or 5×10^4 cells/well for, respectively, immunoblot or microscopy experiments.

Cells were transfected using the jetPEI™ reagent (Polyplus) according to manufacturer's protocol for 24 h.

Immunofluorescence microscopy

Transfected CHO cells cells were fixed for 20 min in 4% PFA (w/v, in PBS) and permeabilized with Saponin 0.1% (v/v, in PBS) for the same time, or with methanol for 5 min at -20ºC (for Rab11 labeling). For labelings, primary antibodies were diluted in PBS with 10% horse serum and incubated for 1 h, followed by PBS washing and incubation with appropriate seconday antibodies in the same conditions.

Primary antibodies used were anti-myc (mouse, Clone 9E10, Calbiochem; 1:200), anti-Rab5 (rabbit, Abcam ab218624; 1:50), anti-Rab6 (rabbit, Santa Cruz Biotechnology; 1:50), anti-Rab7 (rabbit, Santa Cruz Biotechnology; 1:50) or anti-Rab11 (rabbit, Santa Cruz Biotechnology; 1:50) and secondary antibodies were fluorophore-conjugated antibodies anti-mouse-AlexaFluor350, anti-rabbit-AlexaFluor488 or anti-mouse-AlexaFluor560 (Jackson ImmunoResearch; 1:200). DNA labeling was carried out with 4,6-Diamidino-2-phenylindole (DAPI; 1:30,000), and actin staining was carried out by incubation with Phalloidin-Alexa555 (Thermo Fisher Scientific, 1:200) during 30 min. Images were acquired on an Axio Imager D2 (Zeiss) or a Laser Scanner Confocal Microscope Zeiss LSM710 (for quantification of colocalization) and processed with ImageJ 2.14 software. Quantitative analysis of co-localization between VipA and FYVE-GFP was performed by calculating the Manders overlap coefficient, corresponding to the fraction of red pixels (VipA signal) that overlaps with green pixels (FYVE-GFP) in relation to the total red pixels. For this purpose, signal intensities for each cell ($n \geq 12$, two independent experiments) were processed in ImageJ and the coefficients determined with the plugin JACoP [27]. Statistical analysis was performed using GraphPad Prism software version 5.02. P-values were calculated using a t-test (unpaired, two tails).

Co-immunoprecipitation assays

CHO cells were transfected with pEGFP-N1, plasmids encoding EGFP-Rab5 variants, pEF6a and plasmids encoding VipA-myc variants using the jetPEI™ transfection reagent (Polyplus) according to manufacturer's protocol. Cells were harvested 24 h post transfection and co-immunoprecipitations performed using Chromotek GFP-Trap agarose beads essentially as described by the manufacturer. In brief, cells were lysed with Lysis Buffer (50 mM Tris–HCl pH 8, 150 mM NaCl, 0.1 mM EDTA, 0.5% [w/v] IGEPAL$^{\grave{O}}$ CA-630, 1 mM dithiothreitol [DTT], 100 µg/ml phenylmethylsulfonyl fluoride [PMSF] and a protease Inhibitor cocktail [Amresco]), and the beads were incubated with lysate-supernatants for 4 h at 4 °C in dilution buffer (50 mM Tris–HCl pH 8, 150 mM NaCl, 0.1 mM ethylenediaminetetraacetic acid [EDTA], 1 mM DTT, 100 µg/ml PMSF and a protease Inhibitor cocktail [Amresco]), and washed three times with wash buffer (50 mM Tris–Hcl pH 8, 150 mM NaCl, 0.1 mM EDTA). Aliquots of input, non-bound, washes and bound samples were analyzed by immunoblotting (see below).

SDS-PAGE and immunoblotting

For SDS-PAGE, samples containing 1 × Laemmli buffer were boiled for 5 min and ran on 12% gels at 150 V for 75 min. Gels were processed for immunoblotting using Trans-Blot Turbo Transfer System (BioRad) and 0.2 µm pore-size nitrocellulose membranes (BioRad). Membranes were incubated 1 h with primary antibodies diluted 1:1000 in Blocking solution (PBS with 0.1% Tween [v/v] and 4% [w/v] non-fat milk powder; goat anti-GFP, SICGEN; rabbit anti-VipA; mouse anti-myc, Clone 9E10, Calbiochem), followed by PBS washing and incubation with appropriate secondary antibodies in the same conditions (anti-goat or anti-mouse horseradish peroxidase (HRP)-conjugated secondary antibodies, GE Healthcare or Jackson ImmunoResearch; 1:10,000). For VipA-lipid interaction, PIP strips membranes (Echelon Biosciences) were incubated with 5 mg of purified His_6-VipA in Blocking solution and hybridation carried out as above. Immunoblot detection was done with Western Lightning ECL Pro (Perkin Elmer) and exposure to Amersham Hyperfilm ECL (GE Healthcare).

Overexpression and purification of His_6-VipA and GST-Rab5 proteins

E. coli BL21(DE3) strains harboring plasmids encoding 6xHis-tagged proteins (see Table S1) were grown at 37 °C for 18 h (His_6-VipA and His_6-$VipA_{\Delta NH2}$) or at 37 °C for 5 h followed by 24 h at 26 °C (His_6-$VipA_{\Delta COOH}$) in auto-induction conditions [28]. Cells were harvested by centrifugation and the cell pellet was resuspended in 10 ml of lysis buffer (50 mM Na_2HPO_4, 300 mM NaCl, 20 mM imidazole). Bacteria were lysed with 3 passages in a French press at 900 PSI in the presence of 1 mM PMSF and lysates were centrifuged at 13,000 xg for 30 min at 4°C. His-tagged proteins were purified from the soluble fraction using Ni–NTA (nickel-nitrilotriacetic acid) chromatography (Qiagen) and eluted with Imidazole gradients. For purification of GST-Rab5 proteins (GST-$Rab5^{WT}$, GST-$Rab5^{CA}$ or GST-$Rab5^{DN}$), the corresponding strains were grown in LB and overexpression induced for 4 h by addition of 1 mM IPTG. Bacteria were then pelleted, resuspended in PBS and lysed

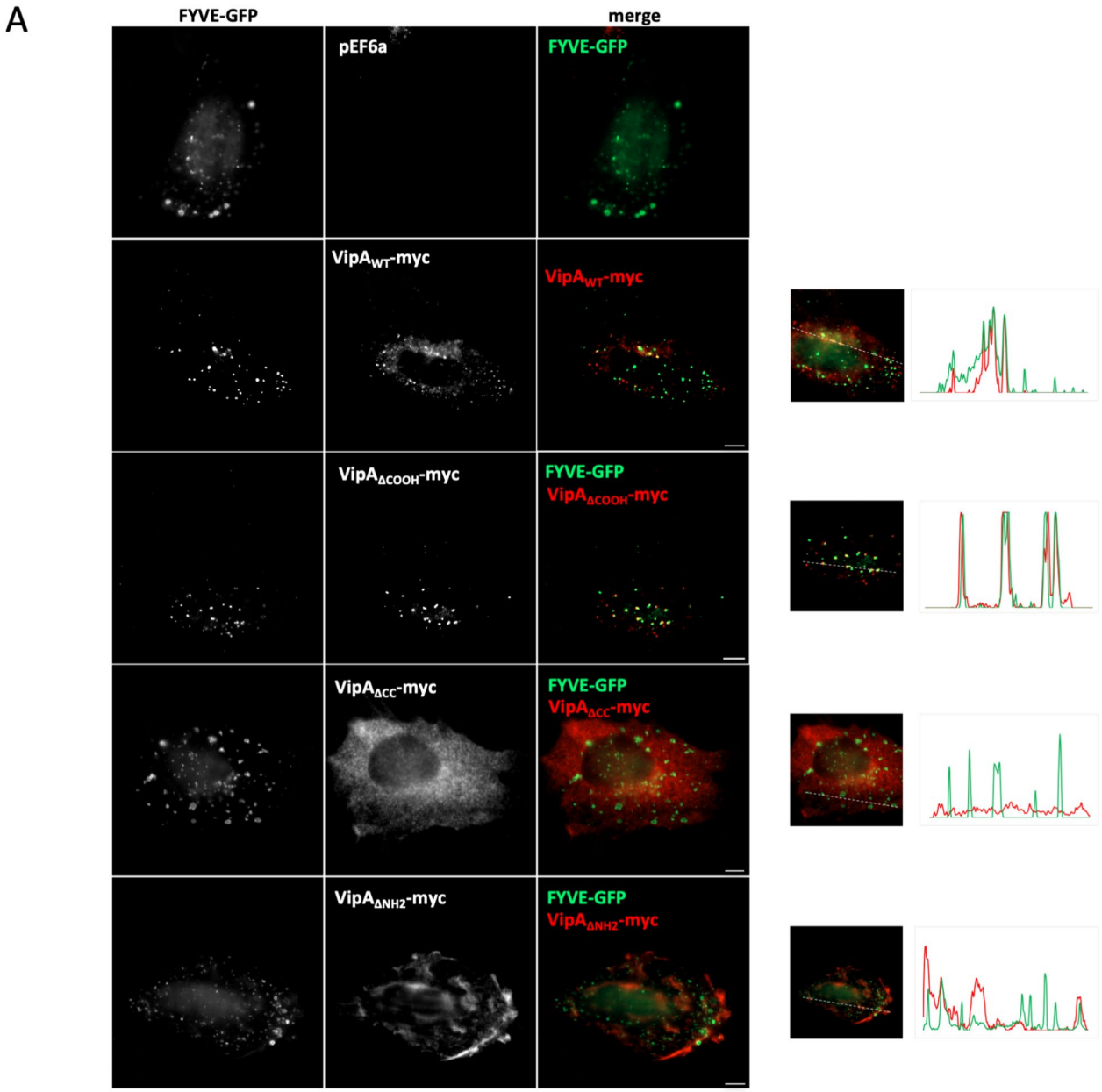
A
FYVE-GFP
pEF6a
merge
FYVE-GFP
VipA$_{WT}$-myc
VipA$_{WT}$-myc
VipA$_{\Delta COOH}$-myc
FYVE-GFP
VipA$_{\Delta COOH}$-myc
VipA$_{\Delta CC}$-myc
FYVE-GFP
VipA$_{\Delta CC}$-myc
VipA$_{\Delta NH2}$-myc
FYVE-GFP
VipA$_{\Delta NH2}$-myc

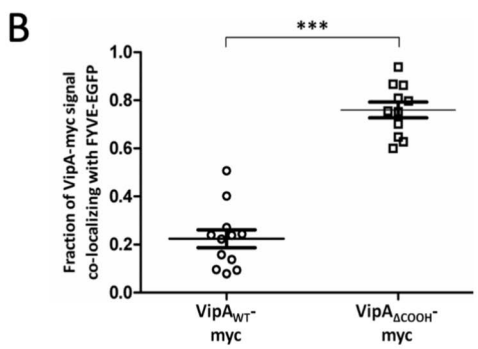
B
***
Fraction of VipA-myc signal co-localizing with FYVE-EGFP
1.0
0.8
0.6
0.4
0.2
0.0
VipA$_{WT}$-myc
VipA$_{\Delta COOH}$-myc

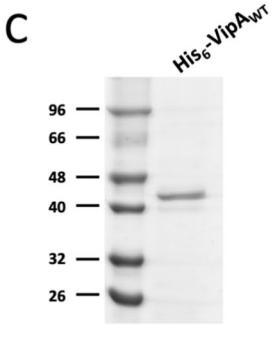
C
His$_6$-VipA$_{WT}$
96
66
48
40
32
26

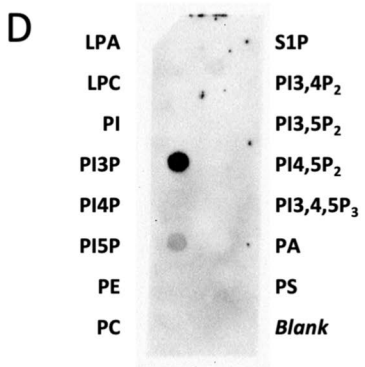
D
LPA
LPC
PI
PI3P
PI4P
PI5P
PE
PC
S1P
PI3,4P$_2$
PI3,5P$_2$
PI4,5P$_2$
PI3,4,5P$_3$
PA
PS
Blank

Fig. 1 *L. pneumophila* effector VipA interacts with lipid PI3P in CHO cells and in vitro. **A** CHO cells were cotransfected with plasmid pEF6a derivatives encoding myc-tagged versions of VipA (wild-type, $VipA_{WT}$; lacking aminoacid residues 207–339, $VipA_{\Delta COOH}$; lacking aminoacid residues 134–206, $VipA_{\Delta CC}$; or lacking aminoacid residues 1–133, $VipA_{\Delta NH2}$; in red), and plasmid pEGFP-N1 derivatives encoding GFP or FYVE-GFP (in green). Cells were fixed with 4% PFA, permeabilized with 0.1% Triton-X and labeled with an anti-myc antibody (mouse) and secondary anti-mouse-Rhodamine. Microscopy was performed on a Laser Scanner Confocal Microscope (Zeiss LSM710). Representative images are shown (left) and corresponding Profile Plots for the intensity of FYVE-GFP and VipA were performed with ImageJ (right). Scale bars, 10 µm. **B** Quantification of colocalization was performed for $VipA_{WT}$ and $VipA_{\Delta COOH}$ by determining the fraction of the effector overlapping with FYVE-GFP in each cell (Manders coefficient). Bars correspond to mean and standard error of the mean; ***$P<0.001$. **C** Coomassie stained SDS-PAGE with 2.2 ug of Ni–NTA purified His_6-$VipA_{WT}$. **D** Membrane containing the indicated immobilized lipids was incubated with purified His_6-VipA and probed with polyclonal anti-VipA (rabbit) and secondary anti-rabbit-HRP (goat) antibodies. LPA, Lysophosphatidic Acid; LPC, Lysophosphocholine; PI, PhosphatidyInositol; PI3P, PhosphatidyInositol 3-Phosphate; PI4P, PhosphatidyInositol 4-Phosphate; PI5P, PhosphatidyInositol 5-Phosphate; PE, Phosphatidylethanolamine; PC, Phosphatidylcholine; S1P, Sphingosine-1-phosphate; $PI3,4P_2$, PhosphatidyInositol 3,4-Bisphosphate; $PI3,5P_2$, PhosphatidyInositol 3,5-Bisphosphate; $PI4,5P_2$, PhosphatidyInositol 4,5-Bisphosphate; $PI3,4,5P_3$, PhosphatidyInositol 3,4,5-trisphosphate; PA, Phosphatidic Acid; PS, Phosphatidylserine

as above. Proteins were purified by loading the soluble fractions on glutathione-sepharose columns and elution with 10 mM glutathione in PBS. Where indicated, loading of Rab5 with with GTPgS, a non-hydrolysable form of GTP, was carried out essentially as described [29] with the following alterations. Purified GST-Rab5 was incubated for 30 min at room temperature with 2 ml of Nucleotide Exchange Buffer (20 mM HEPES pH 7.5, 100 Mm NaCl, 10 mM EDTA, 5 mM $MgCl_2$, 1 mM DTT) containing 1 mM GTPγS (Jena Bioscience) in a final 3 µM GST-Rab5 concentration. The reaction mixture was transferred to a 6 ml Centrifugal Concentrator column (MWCO 10 kDa, Vivaspin), subjected to two centrifugation cycles at 4 °C and 5000 × *g* for 2 min. Then, 2 ml of Nucleotide Stabilization Buffer supplemented with 10 µM of GTPγS were loaded into the column, which was centrifuged twice at 4 °C, 5000 × *g* for 2 min, and once at 2,000 × g for 2 min. The remaining ~ 200 µl of protein solution was recovered and stored at −20 °C until further use.

Bacterial two-hybrid assays

The bacterial adenylate cyclase two-hybrid (BACTH) system [42] (Euromedex) was used. This system includes four plasmids (pUT18, pUT18C, pKNT25 and pKT25; Table S1) enabling fusions to the N- or C-terminus of T18 or T25 fragments of the catalytic domain of adenylate cyclase (CyaA) from *Bordetella pertussis*. For bacterial two-hybrid, adenylate cyclase (Cya)-deficient *E. coli* BTH101 was transformed with plasmids expressing the different T18 and T25 hybrid proteins. Qualitative screening of putative interactions was firstly made on plates by growing co-transformants on solid LB supplemented with isopropyl β-D-1-thiogalactopyranoside (IPTG; 0.5 mM), the chromogenic substrate 5-bromo-4-chloro-indolyl-β-D-galactoside (X-gal; 40 µg/ml) and appropriate antibiotics. Plates were incubated for 24 h at 28 °C. Quantification of β-gal activity was accomplished by monitoring the β-gal-dependent cleavage of *ortho*-nitrophenyl-β-galactoside (ONPG) into the colorimetric molecule *ortho*-nitrophenol, as described by the manufacturer (Euromedex). In all experiments, we used as positive control strain BTH101 transformed with plasmids pUT18C-zip and pKT25-zip, encoding two leucine zipper domains, and the indicated negative control strains. The final results were based on at least three independent experiments, using three different colonies. Statistical significance was assessed using a student t-test as indicated.

In vitro actin polymerization assays

Preparation of G-Actin and polymerization assays were carried out essentially as described [30] with the following alterations. Samples contained 3 µM G-actin (Cytoskeleton, > 99% pure; 20% Pyrene-actin) and purified His_6-VipA mutants in G-Mg buffer were added as indicated. Polymerization assays were carried out in quartz cuvettes (3 mm optical path length), and fluorescence read in a Varian Cary Eclipse fluorescence reader. Values were obtained using an excitation wavelength of 365 nm and emission of 407 nm (10 nm slit width) and recorded at 1 min intervals. Data were collected with Cary Eclipse software and then processed in Excel (Microsoft).

For quantification of the number of filaments by microscopy, handmade flowcells were prepared as a sandwich of a glass slide (1.0–1.2 mm thick, Fisherbrand) with two Parafilm strips placed longitudinally over it with an approximately 15 mm wide channel between them and a glass coverslip (20 × 20 mm, Menzel-Gläser) on top. This set was heated at 100 °C to melt the parafilm. Liquid was introduced using a micropipette on one end of the channel and pulled through the flow cell by using an absorptive cloth on the other end. Before sample introduction, the flow cells were incubated with 50 µl of 10% (w/v) BSA for 10 min to reduce non-specific adsorption of actin to the surfaces of the glass. Flow cells were washed with 90 µl of G-buffer (1 mM Tris–HCl pH 7.8, 0.2 mM $CaCl_2$, 0.5 mM DTT, 0.2 mM Mg-ATP) and then 20 µl of filamin (0.1 mg/ml, from turkey smooth muscle, Hypermol) was applied as tethering protein and left to incubate for 5 min. Finally, flow cells were washed again with 90 µl of G-buffer.

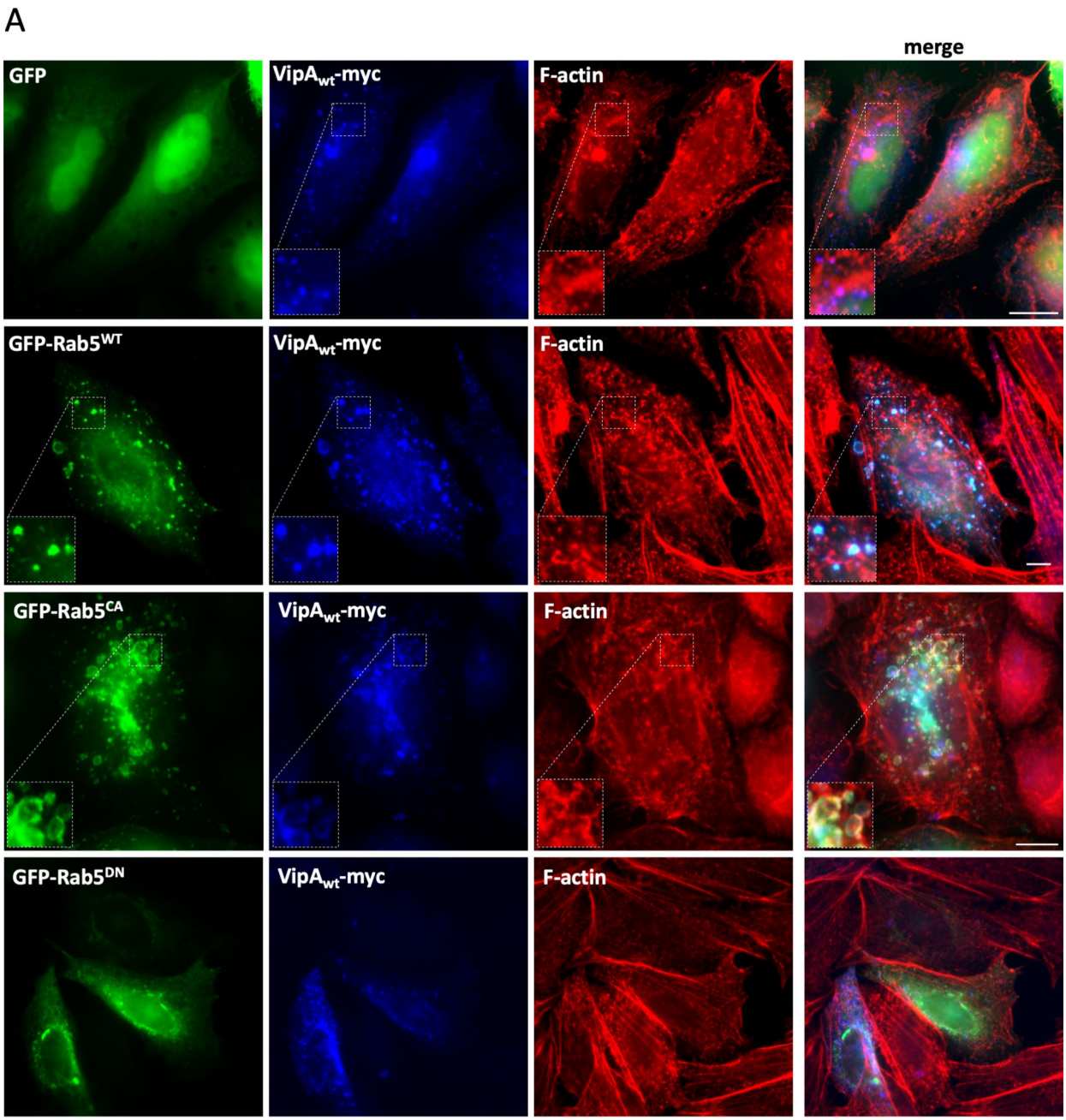
A
merge
GFP
VipA$_{wt}$-myc
F-actin
GFP-Rab5^{WT}
VipA$_{wt}$-myc
F-actin
GFP-Rab5^{CA}
VipA$_{wt}$-myc
F-actin
GFP-Rab5^{DN}
VipA$_{wt}$-myc
F-actin

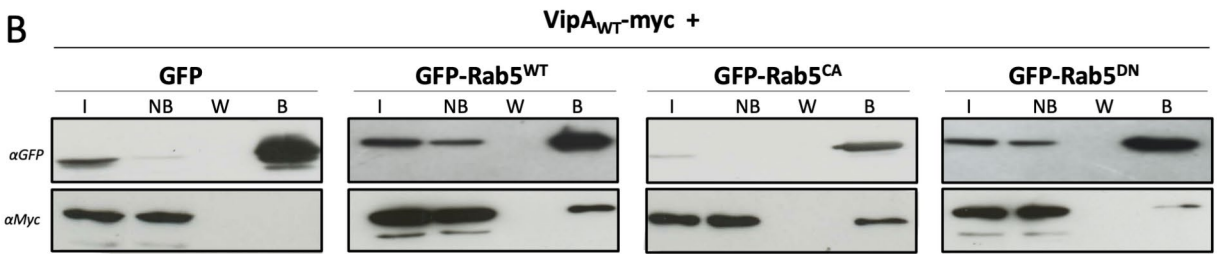
B
VipA$_{WT}$-myc +
GFP
GFP-Rab5^{WT}
GFP-Rab5^{CA}
GFP-Rab5^{DN}
I NB W B
αGFP
αMyc

Fig. 2 *L. pneumophila* VipA interacts with Rab5 in CHO cells. Cells were cotransfected with plasmids encoding full-length VipA-myc and wildtype or Rab5 mutants ($Rab5^{WT}$, $Rab5^{CA}$ or $Rab5^{DN}$; GFP tagged, in green). **A** Cells were fixed with 4% PFA and permeabilized with 0.1% Triton-X; VipA was labeled with an anti-myc antibody (mouse) and secondary anti-mouse-Alexa Fluor 350 (in blue), and F-actin with Phalloidin-Alexa Fluor 555 (red). **B** For co-immunoprecipitation assays, cells were lysed and used in GFP-trap assays. Samples of Input (I), Non-bound (NB), final Wash (W) and Bound (B) fractions were separated by SDS-PAGE. Immunoblots were carried out using anti-GFP (goat) or anti-myc (mouse) antibodies followed by corresponding secondary HRP-labeled secondary antibodies

In vitro actin polymerization reactions were performed as follows: 100 nM Atto488-Actin (α-skeletal muscle actin from rabbit skeletal muscle, Hypermol) was incubated for 5 min on ice with G-buffer and 5% (v/v) of 10 × ME buffer (4 mM $MgCl_2$, 20 mM EGTA) to exchange Ca^{2+} and Mg^{2+}. His_6-VipA, GST-Rab5 and G-buffer were then added to a final volume of 100 µl. Reactions were initiated by introducing 10 × KMEI (500 mM KCl, 20 mM $MgCl_2$, 20 mM EGTA, 300 mM imidazole) and 40% (v/v) of Imaging Buffer (40 mg/ml catalase from bovine liver, 1.8 mg/ml glucose oxidase from *Aspergillus niger*, 100 mM a-D-glucose, 2.5% [v/v] β-mercaptoethanol, 0.5% [w/v] methylcellulose). After introducing the different components for each sample, both open ends of the channel were sealed with grease (korasilon-paste, GmbH).

Widefield imaging was done on a Leica DMI6000 inverted microscope, using illumination from a Leica EL6000 source, a fluorescence filter cube with the Leica GFP ET filter set, a 100x/1.46 a-plan apochromat oil immersion objective plus a 1.6 × magnifier, Leica type F immersion oil, and an Evolve 512 electron microscopy charge-coupled device (EM-CCD) camera (Photometrics) using 16-bit EM gain amplification. The final pixel size was 100 nm. To assess actin polymerization over time, one-hour time-lapse videos were obtained starting five minutes after sample preparation. To evaluate nucleation at early time points with higher number of images, at least 20 images of different fields of view were acquired for every sample five minutes after sample preparation. To automatically quantify the number of actin filaments, fluorescence images were segmented using DeLTA [31], using model weights that we obtained from training the DeLTA neural network on manually segmented training data. Binary images were then processed using the Ridge Detection plug-in in ImageJ (https://imagej.net/plugins/ridge-detection) to obtain the number and lengths of filaments in individual images. This data was then analyzed and plotted using custom Python scripts.

Results

VipA interacts with the early endosome membrane lipid PI3P

Our previous results showed a partial localization of VipA to early endosomes when ectopically expressed in mammalian epithelial cells and when delivered into THP-1 macrophages during infection by *L. pneumophila* [25, 30]. To gain insight into the function of VipA in these organelles, we were interested in finding its molecular target(s) therein. Two key identifiers of early endosomes are the lipid PI3P and the small GTPase Rab5, fundamental in the maturation process of these organelles [32]. We initially assessed a possible association with PI3P by observing the localization of ectopically expressed VipA-myc and the PI3P probe 2xFYVE-GFP in cotransfected CHO cells, a reliable model to mimic VipA localization observed during infection [25]. We observed a partial overlap between vesicles enriched in PI3P ($PI3P^+$ vesicles) and $VipA_{WT}$ puncta (Fig. 1A, overlap profile on the right), similarly to what we had observed in previous work with vesicles enriched in EEA1 ($EEA1^+$) vesicles [30].

To find the region of VipA involved in this process, we used VipA-myc constructs previously characterized [30], either lacking the NH_2-terminal region (mutant $VipA_{\Delta NH2}$, deletion of amino acid residues 1–133), the central coiled-coil region ($VipA_{\Delta CC}$; lacking a.a. 134–205), or the COOH-terminal/actin-binding region ($VipA_{\Delta COOH}$; missing a.a. 206–339). Deletion of the actin-binding region of VipA led to a conspicuous association of $VipA_{\Delta COOH}$ with $PI3P^+$ vesicles, reflected in the overlay of intensity profile plots for both signals (Fig. 1A, right). In contrast, removal of the NH_2-terminal or coiled-coil regions caused a loss of the typical VipA puncta, leading to a mostly cortical localization for $VipA_{\Delta NH2}$ and cytosolic distribution for $VipA_{\Delta CC}$ and no obvious colocalization with FYVE-GFP (Fig. 1A, bottom panels). In the case of the two VipA variants displaying discernible colocalization with PI3P, $VipA_{WT}$ and $VipA_{\Delta COOH}$, the degree of colocalization was quantified by determining the fraction of VipA overlappping with FYVE-GFP in each cell (Manders coefficient). Confirming the previous visual examinations, the average degree of colocalization of $VipA_{\Delta COOH}$ with PI3P was 76%, significantly higher than the 22% found for $VipA_{WT}$ (Fig. 1B).

To validate the specificity of the association between VipA and PI3P we next performed in vitro lipid-protein

interaction assays. For this, we incubated a membrane containing spots of different immobilized phosphoinositide lipids with purified histidine-tagged VipA (His_6-$VipA_{WT}$; Fig. 1C). Subsequent detection with anti-VipA antibodies revealed the direct interaction of the effector with PI3P, and residually with PI5P, but not with the remaining membrane lipids (Fig. 1D). In these assays, $VipA_{\Delta CC}$ and $VipA_{\Delta COOH}$ bound PI3P in a manner comparable to $VipA_{WT}$, whereas $VipA_{\Delta NH2}$ displayed broader, apparently non-specific binding to multiple phosphoinositides (Supplemental Figure S1). These results suggest that the NH_2-terminal region of VipA is important for conferring specificity toward PI3P.

Together, colocalization of VipA with $PI3P^+$ vesicles in CHO cells and its direct binding to PI3P in vitro show that VipA interacts specifically with endosomal lipid PI3P.

VipA interacts with GTPase Rab5

A subset of early endosomal proteins that bind directly PI3P, including EEA1, also interact with Rab5 [32, 33]. Thus, we decided to also test the association of VipA with this small GTPase. As above, CHO cells were transfected with plasmid encoding $VipA_{WT}$-myc and endogenous Rab5 labeled with anti-Rab5 antibodies. A clear colocalization of VipA with Rab5 was observed (Fig. S2), but not with endogenous Rab6 (a Golgi GTPase), Rab7 (late endosomes/lysosomes), Rab11 (recycling endosomes) or plasmid encoded YFP-Rab4 (early/recycling endosomes). Next, to analyze if this localization of VipA depended on the active or inactive state of Rab5 GTPase, we cotransfected cells additionally with plasmids encoding GFP or GFP-tagged Rab5a variants. In cells overexpressing GFP-Rab5 we observed the formation of enlarged vesicles enriched in Rab5 ($Rab5^+$ endosomes) due to excessive homotypic fusion of early endosomes, as previously reported (Fig. 2A) [34]. In addition, in these cells there was a change in the localization of VipA to the larger endosomes enriched in Rab5, instead of the smaller VipA puncta seen in cells producing GFP alone (Fig. 2A). To examine a possible preference of VipA to the active/GTP-bound or to the inactive/GDP-bound form of Rab5, we expressed two well-characterized GTPase mutants that mimic these two activation states. Mutant $Rab5^{Q79L}$ is locked in its GTP-bound conformation and is therefore constitutively active (henceforth named $Rab5^{CA}$) whereas $Rab5^{S34N}$ is an inactive dominant-negative mutant ($Rab5^{DN}$) [15, 35]. When $Rab5^{CA}$ was present, as observed above for cells overexpressing GFP-Rab5, VipA changed its localization from small widespread puncta to the typical enlarged endosomes resulting from the activity of this active GTPase (Fig. 2A). These endosomes are enriched in actin filaments, independently of the presence of VipA (magnified insets displayed for comparison, Fig. 2A). In contrast, inactive $Rab5^{DN}$ is mostly dispersed in the cytosol with some enrichment in the perinuclear region. In cells expressing $Rab5^{DN}$, the striking redistribution of VipA mirroring the localization of the $Rab5^{DN}$ was not as evident, although in some cells accumulation of VipA puncta in the perinuclear zone was apparent (Fig. 2A).

A possible interaction between VipA and Rab5 suggested by their subcellular co-localization was tested by co-immunoprecipitation assays. For this, we used the previous experimental setup (i.e. CHO cells co-expressing $VipA_{WT}$-myc and GFP-Rab5 variants) and immunoprecipitated GFP tagged proteins from cell lysates using GFP-Trap beads (Chromotek). After separation by SDS-PAGE, samples were subjected to immunoblots with anti-myc and anti-GFP antibodies, to assess the presence of VipA in fractions with immunoprecipitated Rab5. VipA was detected in fractions containing GFP-$Rab5^{WT}$, GFP-$Rab5^{CA}$ and, to a much lesser extent, GFP-$Rab5^{DN}$, but not in a sample with GFP alone (Fig. 2B).

Collectively, results from colocalization experiments and co-immunoprecipitation assays show that ectopically expressed VipA forms a complex with Rab5 in mammalian cells, particularly with active forms of the GTPase.

Interaction of VipA with Rab5 in vivo is direct and is mediated by the NH_2-terminal region

To identify the region of VipA necessary for its association to Rab5, CHO cells were co-transfected with the constructs producing myc-tagged $VipA_{\Delta COOH}$, $VipA_{\Delta CC}$ and $VipA_{\Delta NH2}$ and with the GFP-tagged Rab5 variants ($Rab5^{WT}$, $Rab5^{CA}$, $Rab5^{DN}$). $VipA_{\Delta COOH}$ showed a similar localization to $VipA_{WT}$ in cells producing GFP alone and when co-expressed with the Rab5 versions, as its localization was altered from small puncta to larger organelles, distinctively overlapping with vesicles containing $Rab5^{WT}$ and $Rab5^{CA}$ (Fig. 3A, top panel). In agreement, co-immunoprecipitation assays confirmed the ability of $VipA_{\Delta COOH}$ to form a complex with Rab5 in cells (Fig. 3B, top panel). Deletion of the coiled-coil region and particularly of the NH_2-terminal region of VipA abrogated this association, as $VipA_{\Delta NH2}$ is absent in Rab5 immunoprecipitated fractions and its subcellular localization remains mostly cytosolic in the presence of the Rab5 variants (Fig. 3A, B, bottom panels).

To further validate the interaction of VipA with Rab5 and rule out the requirement of additional binding partners for the formation of a Rab5-VipA complex, we used a Bacterial Two-Hybrid System (BACTH; Euromedex). This methodology is based on *Bordetella pertussis* adenylate cyclase CyaA being only catalytically active when its two subunits, T18 and T25, are in physical proximity. By expressing fusion proteins containing T18 or T25, interactions

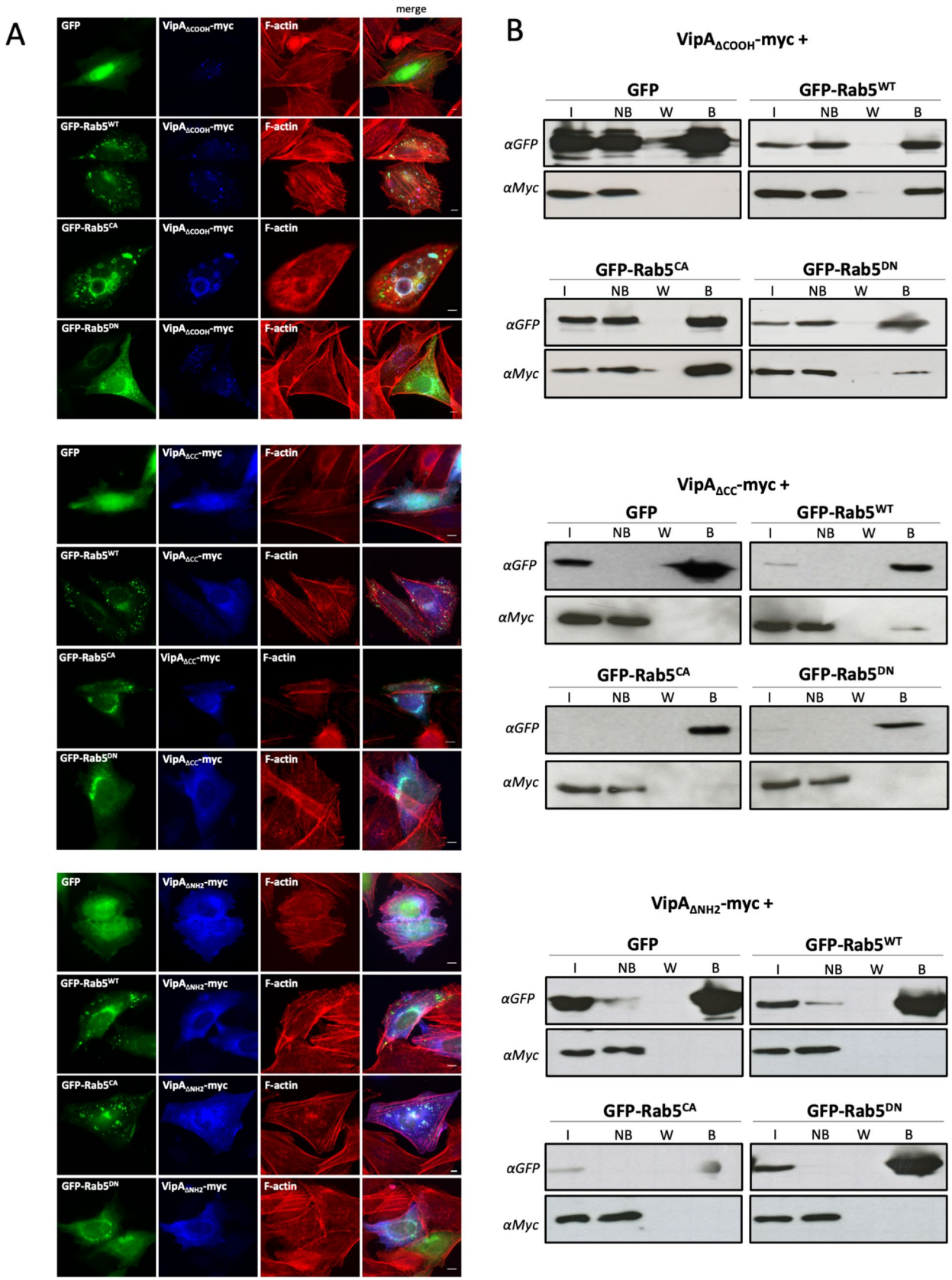

Fig. 3 Interaction between VipA and Rab5 is mediated by the NH_2 region of VipA. CHO cells were cotransfected with plasmids encoding VipA-myc constructs (VipA$_{\Delta COOH}$, VipA$_{\Delta CC}$ and VipA$_{\Delta NH2}$) and wild-type or Rab5 mutants (Rab5^{WT}, Rab5^{CA} or Rab5^{DN}; GFP tagged). Cells were processed for microscopy analysis **A** or co-immunoprecipitation assays **B**, as described in the legend of Fig. 2. Scale bar, 5 µm

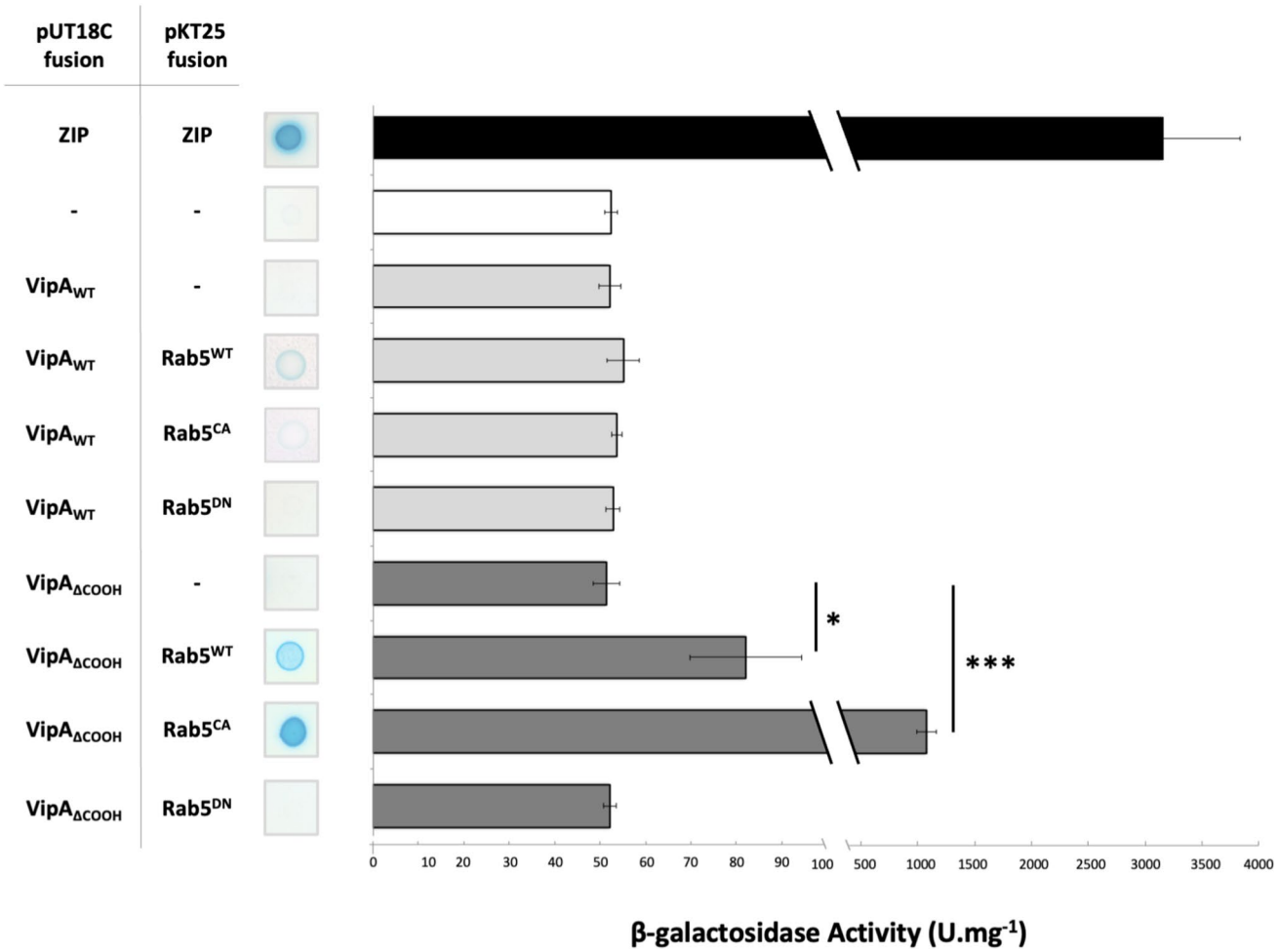

Fig. 4 VipA interacts directly with Rab5 in a Bacterial Two-Hybrid (BACTH) Assay. *E. coli* recipient strain BTH101 was co-transformed with plasmids encoding a Rab5 variant (Rab5^{WT}, Rab5^{CA} or Rab5^{DN}, encoded in plasmid pUT18C) and a VipA variant (VipA$_{WT}$ or VipA$_{\Delta COOH,}$ encoded in plasmid pKT25). A positive control for the BACTH system was used (Zip-Zip interaction, black bar). Negative controls included a strain with the two empty vectors (white bar) and strains expressing a protein under test and the counterpart empty vector. Activity of reporter gene *lacZ* was measured qualitatively by plating in solid media with X-gal (left) or quantitatively by β-galactosidase assays in liquid media (right). Bars and error bars represent the average and standard error of the mean of at least 3 independent experiments. Statistical analysis was made using a Student t-test (*$p<0.05$; ***$p<0.001$)

will activate several reporter genes whose activity can be analyzed in specific culture media. Hence, we constructed plasmids encoding fusion proteins of wild-type VipA or Rab5 to T18 or T25 (Table S1). The reporter strain *E. coli* BTH101 was transformed with plasmid pairs expressing the two putative binding partners, in all possible combinations, and transformants were inoculated on LB plates containing X-gal. We observed a weak but discernible Lac^{+}/blue phenotype for the strain co-expressing T18-VipA/T25-Rab5, suggesting an interaction between the chimeric proteins containing VipA$_{WT}$ and Rab5^{WT} at their COOH-terminal ends (Fig. 4, left). Based on this plasmid/ fusion protein combination (pUT18C-VipA and pKT25-Rab5), we further investigated if complex formation was affected in variants Rab5^{CA} or Rab5^{DN}. A similarly weak interaction was observed with Rab5^{CA}, but not apparent with inactive variant Rab5^{DN}. Interestingly, interaction with Rab5^{WT} and Rab5^{CA} was greatly enhanced when variant VipA$_{\Delta COOH}$ was used, suggesting a possible hindrance exerted by the COOH/actin-binding region in formation of the VipA-Rab5 complex. These results were confirmed by quantification of the β-galactosidase activity in liquid media (Fig. 4, right).

Taken together, the results from microscopy, co-immunoprecipitation and BACTH assays indicate that VipA and Rab5 form a complex in mammalian cells that does not require additional eukaryotic binding partners. The interaction is favored by the active form of Rab5, requires the NH_2-terminal region of VipA but a possible inhibitory mechanism may be conveyed by the COOH-terminal/actin-binding region of VipA.

Active Rab5 inhibits VipA-mediated de novo formation of actin filaments

We then tested a possible effect of the binding of Rab5 to VipA on the ability of VipA to nucleate the polymerization of new actin filaments. In vitro pyrene-actin polymerization assays were performed as previously described [30] in the presence of purified His_6-VipA and the three aforementioned Rab5 variants carrying an NH_2-terminal GST-tag. The capacity of wild-type VipA to drive F-actin polymerization was slightly affected by the presence of $Rab5^{WT}$ (Fig. 5A) and drastically reduced by constitutively active mutant $Rab5^{CA}$ (Fig. 5B), albeit unchanged by inactive GTPase $Rab5^{DN}$ (Fig. 5C). This inhibitory effect of $Rab5^{CA}$ was not observed in the case of $VipA_{\Delta NH2}$ (Fig. 5D), a mutant protein that still retains the ability to polymerize actin filaments. This result suggests the inability of $VipA_{\Delta NH2}$ to interact with Rab5 and is consistent with our colocalization, co-immunoprecipitation and BACTH data, indicating that the Rab5-VipA interaction is mediated by the NH_2-terminal region of VipA.

To confirm that this bulk effect on actin polymerization was due to a decrease in VipA-mediated actin nucleation, we quantified de novo actin filament formation. This was carried out by microscopic analysis and counting the number of filaments polymerized in reactions containing Atto 488-monomeric actin and different concentrations of VipA and Rab5 at different timepoints. In these assays, VipA increased the number of actin filaments in a concentration (0–100 nM) and time-dependent (0–65 min) manner (Fig. 5E), in agreement with its actin nucleator function. To assess the effect of Rab5 on the capacity of VipA to nucleate F-actin de novo, we quantified the number of existing filaments at the earliest measurable timepoint, 5 min. In these conditions, a 50-fold increase in the amount of filaments is observed when 100 nM of VipA is present (Fig. 5E, quantification in Fig. 5F). This reaction was then repeated in the presence of purified GST-$Rab5^{CA}$ or GST-$Rab5^{WT}$ loaded with the GTP analog GTPγS, that locks the GTPase in the active conformation. These Rab5 GTPases did not affect de novo F-actin polymerization, but both reduced by fivefold the ability of VipA to nucleate new filaments (Fig. 5F).

Overall, in vitro actin bulk polymerization assays and quantification of the number of actin filaments show that binding of active Rab5 to VipA strongly reduces this effector's ability to nucleate de novo F-actin polymerization.

Discussion

In this study, we advanced the knowledge of the function of *L. pneumophila* effector VipA by identifying two novel binding partners in eukaryotic cells. Beyond its previously established interaction with actin, we showed that VipA binds to the phospholipid PI3P and the small GTPase Rab5, two critical components of early endosomes. The interaction between VipA and Rab5 is direct and mediated by the NH_2-terminal region of VipA. Furthermore, we observed that binding to the active form of Rab5 inhibits VipA-mediated de novo actin filament formation, unveiling a downstream effect of the VipA-Rab5 interaction.

Rab GTPases, including Rab5, have emerged as key targets of intracellular bacteria. In *L. pneumophila*, a deleterious effect of Rab5 in bacterial replication has been highlighted by gene silencing studies in A549 epithelial lung cells and in bone marrow-derived macrophages [17, 19]. Intriguingly, reports on the presence of Rab5 on the LCV have been divergent. Initial studies with HeLa cells overexpressing Rab5c suggested that phagosomes containing wild-type *L. pneumophila* did not acquire this GTPase [36]. However, later proteomic analyses of the LCV membrane revealed the presence of all Rab5 isoforms in the LCVs of macrophages and model amoeba *Dictyostelium discoideum*, a localization that is at least partially dependent on a functional Icm/Dot T4SS [17, 18].

Previous studies have identified two Icm/Dot effectors as Rab5 regulators. Translocated VipD binds to the GTP-bound active form of Rab5 on early endosomes in the vicinity of the LCV, blocking its interaction with downstream effectors. Together with VipD's phospholipase A1 activity, this interaction disrupts endosomal trafficking, thereby reducing LCV exposure to the endosomal compartment and ultimately preventing *Legionella*'s lysosomal degradation in macrophage cells [22, 23]. Another effector, Lpg0393, functions as guanine nucleotide exchange factor (GEF) for endosomal Rab5, Rab21 and Rab22, although the physiological relevance of this activity during infection remains unclear [24]. Interestingly, in the *L. pneumophila* strain Philadelphia-1 genome, *lpg0393* is located near *vipA* (*lpg0390*), suggesting the existence of a gene cluster encoding effectors involved in modulation of the Rab5 pathway.

Recent insights into VipA's function have been expanded by an Yeast Two-Hybrid screening which identified two potential novel VipA binding partners [37]. The first is the eukaryotic protein CDK4, a serine/threonine kinase crucial for cell cycle progression, fortuitously identified in a screening for effector-effector partners and awaiting additional validation [38]. The second is the *L. pneumophila* metaeffector Lpg2149, previously found to block the activity of effectors MavC and MvcA involved in β-actin u biquitination and

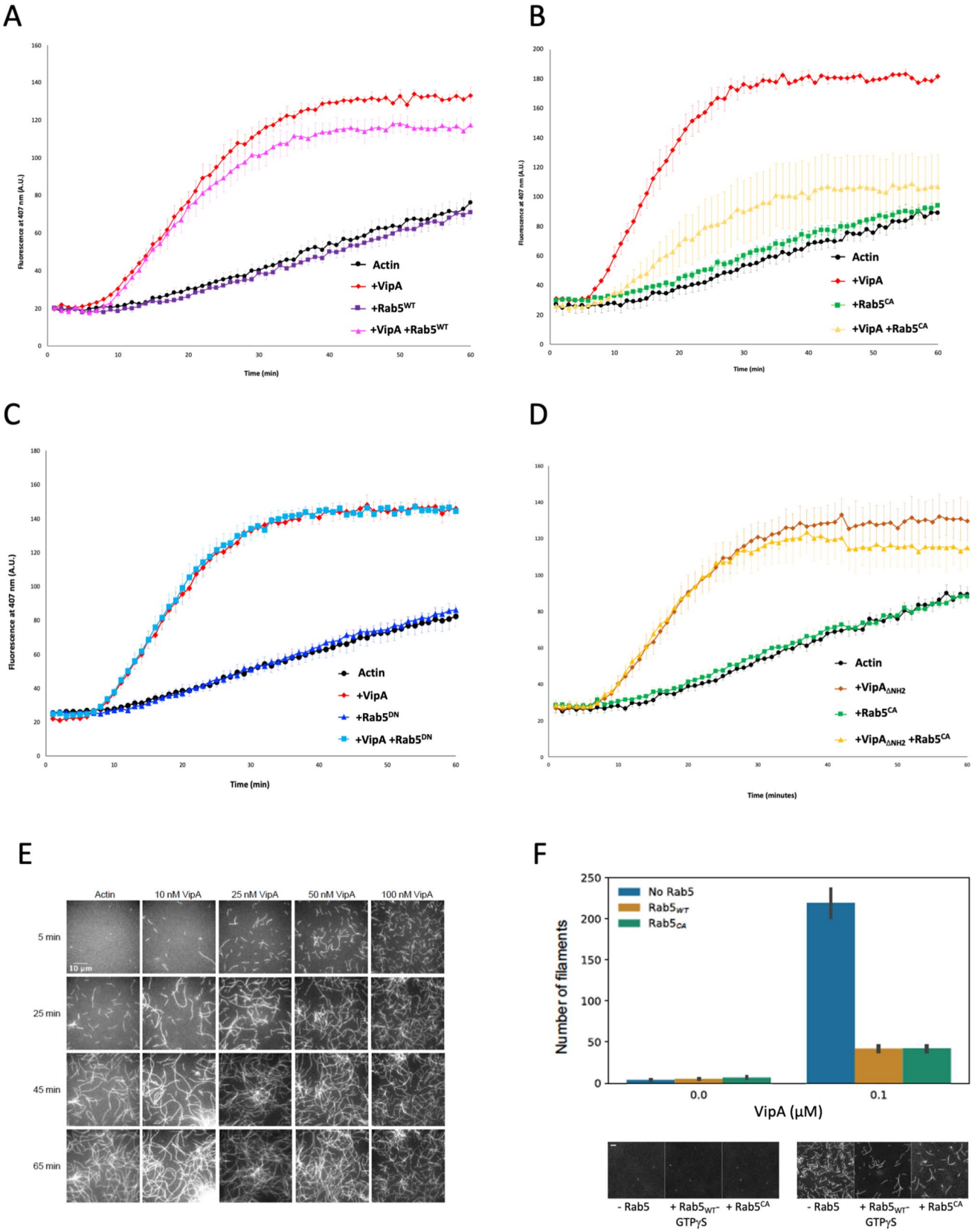
A
Fluorescence at 407 nm (A.U.)
Time (min)
Actin
+VipA
+Rab5WT
+VipA +Rab5WT
B
Fluorescence at 407 nm (A.U.)
Time (min)
Actin
+VipA
+Rab5CA
+VipA +Rab5CA
C
Fluorescence at 407 nm (A.U.)
Time (min)
Actin
+VipA
+Rab5DN
+VipA +Rab5DN
D
Time (minutes)
Actin
+VipAΔNH2
+Rab5CA
+VipAΔNH2 +Rab5CA
E
Actin
10 nM VipA
25 nM VipA
50 nM VipA
100 nM VipA
5 min
25 min
45 min
65 min
10 µm
F
No Rab5
Rab5WT
Rab5CA
Number of filaments
VipA (µM)
- Rab5
+ Rab5WT
+ Rab5CA
GTPγS

Fig. 5 Rab5 inhibits VipA-mediated actin polymerization in vitro. **A-D** In vitro pyrene-actin assays were carried out as described (details in Materials and Methods) in the presence of 3 µM of G-actin (20% pyrene-labeled), in the presence of 500 nM of the indicated variants of purified VipA (His_6-$VipA_{WT}$ or His_6-$VipA_{\Delta NH2}$) and Rab5 (GST-$Rab5^{CA}$, GST-$Rab5^{WT}$ or GST-$Rab5^{DN}$). Results represent the average of three independent assays and error bars the standard error of the mean. **E** Microscopic analysis of actin polymerization in the presence of VipA. Samples contained 100 nM of Atto 488-monomeric actin and the indicated His_6VipA concentrations, and for each condition the same field of view was imaged at 5, 25, 45 or 65 min after reaction start (representative images are shown). **F** Quantitative analysis of the number of actin filaments at 5 min after reaction start, in the absence or presence of 100 nM of VipA, $Rab5^{WT}$ or $Rab5^{CA}$. Results represent the average number of filaments counted in at least 20 fields of view from 3 independent experiments, bars correspond to a 68% confidence interval. Representative images of each condition shown below the corresponding quantification. Scale bar, 10 µm

NFkB activity [39]. Additionally, recent studies by Pillon and co-workers have revealed LegK2-VipA as an effector-effector suppression pair [40]. Although these effectors do not physically interact, deletion of *vipA* rescued the defects in intracellular replication and endosomal escape observed in *ΔlegK2* mutants in *A. castellanii*. Interestingly, a role for VipA in the preceding step of bacterial internalization has also been observed in lung epithelial cells. In infection experiments with filamentous *L. pneumophila*, VipA promoted the elongation of membrane wraps around the bacteria, triggered by adhesion to host cell β1 integrin and E-cadherin receptors facilitating entry [41].

Collectively, these findings reveal a complex network of VipA interactions with both bacterial and eukaryotic proteins, in different cell hosts and various timepoints of infection, underscoring its important and widespread presence in *L. pneumophila*'s interaction with host cells. Additionally, this work provides new mechanistic insights into the modulation of actin dynamics and endocytic trafficking by bacterial effector proteins, as VipA is to date the only known effector to directly interact with actin, Rab5 and PI3P. Further studies are needed to elucidate the specific molecular mechanisms used by VipA to modulate the link between these pathways and ultimately coordinate, alongside other effectors, the manipulation of endolysosomal maturation.

Supplementary Information The online version contains supplementary material available at https://doi.org/10.1007/s00430-026-00871-5.

Acknowledgements This project has been funded by: Fundação para a Ciência e a Tecnologia, I.P. (FCT) Grant PTDC/BIA-MIC/2821/2012 to I.F., FCT National funds in the scope of the project UIDP/04378/2025 (DOI identifier 10.54499/UID/04378/2025) and UID/PRR/04378/2025 (DOI identifier 10.54499/UID/PRR/04378/2025)of the Research Unit on Applied Molecular Biosciences-UCIBIO and the project LA/P/0140/2020 (DOI identifier 10.54499/LA/P/0140/2020)of the Associate Laboratory Institute for Health and Bioeconomy—i4HB. Z.H. is supported by FCT through MOSTMICRO-ITQB (https://doi.org/10.54499/UIDB/04612/2020; https://doi.org/10.54499/UIDP/04612/2020) and LS4FUTURE Associated Laboratory (https://doi.org/10.54499/LA/P/0087/2020). We thank Joana Almeida for the construction of plasmid pJA6.

Author contributions All authors contributed to the study conception and design. Material preparation, data collection and analysis were performed by Joana Saraiva, Joana N. Bugalhão, Teresa Carvalho, Zach Hensel and Irina S. Franco. The first draft of the manuscript was written by Irina S. Franco and all authors commented on previous versions of the manuscript. All authors read and approved the final manuscript.

Funding Open access funding provided by FCT|FCCN (b-on).

Data availability No datasets were generated or analysed during the current study.

Declarations

Conflict of interest The authors declare no conflict of interest.

References

1. Newton HJ, Ang DKY, Van Driel IR, Hartland EL (2010) Molecular pathogenesis of infections caused by *Legionella pneumophila*. Clin Microbiol Rev 23:274–298. https://doi.org/10.1128/CMR.00052-09
2. McDade JE, Shepard CC, Fraser DW et al (1977) Legionnaires' disease: isolation of a bacterium and demonstration of its role in other respiratory disease. N Engl J Med 297:1197–1203
3. Price CTDD, Hanford HE, Al-Quadan T et al (2024) Amoebae as training grounds for microbial pathogens. MBio. https://doi.org/10.1128/mbio.00827-24
4. Swanson MS, Isberg RR (1996) Identification of *Legionella pneumophila* mutants that have aberrant intracellular fates. Infect Immun 64:2585–2594. https://doi.org/10.1128/iai.64.7.2585-2594.1996
5. Berger KH, Isberg RR (1993) Two distinct defects in intracellular growth complemented by a single genetic locus in *Legionella pneumophila*. Mol Microbiol 7:7–19 . https://doi.org/10.1111/j.1365-2958.1993.tb01092.x
6. Gomez-valero L, Rusniok C, Carson D et al (2019) More than 18,000 effectors in the Legionella genus genome provide multiple, Independent combinations for replication in human cells. Proc Natl Acad Sci 116:2265–2273. https://doi.org/10.1073/pnas.1808016116
7. Mondino S, Schmidt S, Buchrieser C (2020) Molecular Mimicry: a Paradigm of Host-Microbe Coevolution Illustrated by Legionella. MBio. https://doi.org/10.1128/mBio.01201-20

8. Mondino S, Schmidt S, Rolando M et al (2020) Legionnaires' disease: state of the art knowledge of pathogenesis mechanisms of *Legionella*. Annu Rev Pathol Mech Dis 15:439–466. https://doi.org/10.1146/annurev-pathmechdis-012419-032742
9. Rolando M, Silvestre CD, Gomez-Valero L, Buchrieser C (2022) Bacterial methyltransferases: from targeting bacterial genomes to host epigenetics. Microlife 3:1–13. https://doi.org/10.1093/femsml/uqac014
10. Yang Y, Mei L, Chen J et al (2023) *Legionella pneumophila*-mediated host posttranslational modifications. J Mol Cell Biol. https://doi.org/10.1093/jmcb/mjad032
11. Shames SR (2023) Eat or Be Eaten: Strategies Used by Legionella to Acquire Host-Derived Nutrients and Evade Lysosomal Degradation. Infect Immun. https://doi.org/10.1128/IAI.00441-22
12. Stenmark H (2009) Rab GTPases as coordinators of vesicle traffic. Nat Rev Mol Cell Biol 10:513–525. https://doi.org/10.1038/nrm2728
13. Christoforidis S, Miaczynska M, Ashman K et al (1999) Phosphatidylinositol-3-OH kinases are Rab5 effectors. Nat Cell Biol 1:249–252. https://doi.org/10.1038/12075
14. Rink J, Ghigo E, Kalaidzidis Y, Zerial M (2005) Rab conversion as a mechanism of progression from early to late endosomes. Cell 122:735–749. https://doi.org/10.1016/j.cell.2005.06.043
15. Stenmark H, Parton RG, Steele-Mortimer O et al (1994) Inhibition of rab5 GTPase activity stimulates membrane fusion in endocytosis. EMBO J 13:1287–1296
16. Zerial M, McBride H (2001) Rab proteins as membrane organizers. Nat Rev Mol Cell Biol 2:107–117. https://doi.org/10.1038/35052055
17. Hoffmann C, Finsel I, Otto A et al (2014) Functional analysis of novel Rab GTPases identified in the proteome of purified Legionella -containing vacuoles from macrophages. Cell Microbiol 16:1034–1052. https://doi.org/10.1111/cmi.12256
18. Urwyler S, Nyfeler Y, Ragaz C et al (2009) Proteome analysis of *Legionella* vacuoles purified by magnetic immunoseparation reveals secretory and endosomal GTPases. Traffic 10:76–87. https://doi.org/10.1111/j.1600-0854.2008.00851.x
19. Anand IS, Choi WY, Isberg RR (2020) Components of the endocytic and recycling trafficking pathways interfere with the integrity of the Legionella -containing vacuole. Cell Microbiol 22(4):e13151 . https://doi.org/10.1073/pnas.2303942120
20. Kim S, Isberg RR (2023) The Sde phosphoribosyl–linked ubiquitin transferases protect the Legionella pneumophila vacuole from degradation by the host. Proc Natl Acad Sci 120(33):e2303942120. https://doi.org/10.1073/pnas
21. Steinbach A, Bhadkamkar V, Jimenez-Morales D et al (2024) Cross-family small GTPase ubiquitination by the intracellular pathogen Legionella pneumophila. Mol Biol Cell 35:ar27. https://doi.org/10.1091/mbc.E23-06-0260
22. Gaspar AH, Machner MP (2014) VipD is a Rab5-activated phospholipase A1 that protects *Legionella pneumophila* from endosomal fusion. Proc Natl Acad Sci U S A 111:4560–4565. https://doi.org/10.1073/pnas.1316376111
23. Ku B, Lee KH, Park WS et al (2012) VipD of *Legionella pneumophila* targets activated Rab5 and Rab22 to interfere with endosomal trafficking in macrophages. PLoS Pathog 8:e1003082. https://doi.org/10.1371/journal.ppat.1003082
24. Sohn YS, Shin HC, Park WS et al (2015) Lpg0393 of *Legionella pneumophila* is a guanine-nucleotide exchange factor for Rab5, Rab21 and Rab22. PLoS ONE 10:1–16. https://doi.org/10.1371/journal.pone.0118683
25. Franco IS, Shohdy N, Shuman HA (2012) The *Legionella pneumophila* effector VipA is an actin nucleator that alters host cell organelle trafficking. PLoS Pathog 8:1002546. https://doi.org/10.1371/journal.ppat.1002546
26. Joiner KA, Fuhrman SA, Miettinen HM et al (1990) Toxoplasma gondii: fusion competence of parasitophorous vacuoles in Fc receptor-transfected fibroblasts. Science 249:641–646. https://www.science.org/doi/10.1126/science.2200126
27. Bolte S, Cordelieres FP (2006) A guided tour into subcellular colocalization analysis in light microscopy. J Microsc 224:213–232. https://doi.org/10.1111/j.1365-2818.2006.01706.x
28. Studier FW (2005) Protein production by auto-induction in high density shaking cultures. Protein Expr Purif 41:207–234
29. Murray JT, Backer JM (2005) Analysis of hVps34/hVps15 interactions with Rab5 in vivo and in vitro. Methods Enzymol 403:789–799. https://doi.org/10.1016/S0076-6879(05)03068-5
30. Bugalhão JN, Mota LJ, Franco IS (2016) Identification of regions within the *Legionella pneumophila* VipA effector protein involved in actin binding and polymerization and in interference with eukaryotic organelle trafficking. Microbiol Open 5:118–133. https://doi.org/10.1002/mbo3.316
31. Lugagne JB, Lin H, Dunlop MJ (2020) Delta: automated cell segmentation, tracking, and lineage reconstruction using deep learning. PLoS Comput Biol 16:1–18. https://doi.org/10.1371/journal.pcbi.1007673
32. Simonsen A, Lippé R, Christoforidis S et al (1998) EEA1 links PI(3)K function to Rab5 regulation of endosome fusion. Nature 394:494–498. https://doi.org/10.1038/28879
33. Gaullier JM, Simonsen A, D'Arrigo A et al (1998) FYVE fingers bind PtdIns(3)P [5]. Nature 394:432–433. https://doi.org/10.1038/28767
34. Bucci C, Parton RG, Mather IH et al (1992) The small GTPase Rab5 functions as a regulatory factor in the early endocytic pathway. Cell 70:715–728. https://doi.org/10.1016/0092-8674(92)90306-W
35. Stenmark H, Valencia A, Martinez O et al (1994) Distinct structural elements of Rab5 define its functional specificity. EMBO J 13:575–583 . https://doi.org/10.1002/j.1460-2075.1994.tb06295.x
36. Clemens DL, Lee B, Horwitz MA et al (2000) Deviant Expression of Rab5 on Phagosomes Containing the Intracellular Pathogens Mycobacterium tuberculosis and Legionella pneumophila Is Associated with Altered Phagosomal Fate. Infect immun 68:2671–2684 . https://doi.org/10.1128/iai.68.5.2671-2684.2000
37. Mount C, Urbanus ML, Sheykhkarimli D et al (2024) A comprehensive two-hybrid analysis to explore the L. pneumophila effector-1 effector interactome. MSystems. https://doi.org/10.1101/2024.03.29.587239
38. Baker SJ, Poulikakos PI, Irie HY et al (2022) CDK4: a master regulator of the cell cycle and its role in cancer. Genes Cancer 13:21–45. https://doi.org/10.18632/genesandcancer.221
39. Valleau D, Quaile AT, Cui H et al (2018) Discovery of Ubiquitin deamidases in the pathogenic arsenal of *Legionella pneumophila*. Cell Rep 23:568–583. https://doi.org/10.1016/j.celrep.2018.03.060
40. Pillon M, Michard C, Baïlo N et al (2024) Dual control of host actin polymerization by a *Legionella* effector pair. Cell Microbiol. https://doi.org/10.1155/2024/8896219
41. Prashar A, Ortiz ME, Lucarelli S et al (2018) Small Rho GTPases and the effector VipA mediate the invasion of epithelial cells by filamentous *Legionella pneumophila*. Front Cell Infect Microbiol 8:1–19. https://doi.org/10.3389/fcimb.2018.00133
42. Karimova G, Ullmann A, Ladant D. A bacterial two-hybrid system that exploits a cAMP signaling cascade in Escherichia coli. MethodsEnzymol. 2000;328:59 73. PMID: 11075338. https://doi.org/10.1016/j.ymeth.2012.07.018